

Tuning the $0-\pi$ Josephson junction with a high spin molecule: Role of tunnel contacts, exchange coupling, electron-electron interactions and high spin states

Subhajit Pal and Colin Benjamin*

School of Physical Sciences, National Institute of Science Education & Research, HBNI, Jatni-752050, India

We propose Josephson junction with a high spin molecule sandwiched between two superconductors. This system shows a π junction behavior as a function of the spin magnetic moment state of the molecule, the interface transparency, exchange coupling and electron-electron interactions in the system. The system is theoretically analyzed for possible reason behind the π shift. The crucial role of spin flip scattering is highlighted. Possible applications in quantum computation of our proposed tunable high spin molecule π junction is underscored.

I. INTRODUCTION

High spin molecules(HSM) have great significance in molecular spintronics. They were discovered two decades back¹ and the main purpose of research with these molecules is to design “single molecule magnets”. These molecules, e.g., $Mn_{12}-ac$ has a large ground state spin $S = 10$, with a very slow relaxation of magnetization at low temperatures². These molecules not only possess integer spin but there are a number of high spin molecules which exhibit large half-integer spins like Mn_4O_3 complex³ with $S = 9/2$ and Fe_{19} -complex⁴ with a spin of $S = 33/2$. The reason we are interested in tunable $0-\pi$ Josephson junction is because of the potential applications of this device as a cryogenic memory element which is an important component of a superconducting computer which would be much more energy efficient than supercomputers⁵⁻⁷ based on current semiconductor technology. Further π junction are in high demand as the basic building blocks of a quantum computer⁸.

In this work, we show that a HSM sandwiched between two s-wave superconductors can transit from a 0 to π Josephson junction via tuning any one of the system parameters like strength of tunnel contact, the spin S or magnetic moment of HSM or the exchange coupling J . Our motivation for looking at this set up stems from the fact that most of the π junction proposals depend on either ferromagnet or d-wave superconductor^{9,10} for their functioning. Integrating Ferromagnets into current superconductor circuit technology hasn't been easy. Controlling Ferromagnets is an onerous task. Further d-wave superconductor, in effect high T_c superconductors also have a poor record of being integrated into current superconductor technology. Thus, in this work we obviate the need for any Ferromagnets or d-wave superconductors by implementing a Josephson π junction with a magnetic impurity. This magnetic impurity can be an effective model for a spin flipper or even a high spin molecule.

Our paper is organized as follow- in section II, we introduce our model, give a theoretical background to our study with Hamiltonian, wavefunctions and boundary conditions to calculate the Josephson current. In section III, we use the Furusaki-Tsukuda formalism to calculate the total Josephson current. To calculate the individual contribution-(i)the bound state we take the derivative of bound state energy with respect to phase difference and (ii) for the continuum contributions use the formalism developed in references 11 and 12. Following this we plot the Andreev bound states as a function of phase difference for different values of spin and magnetic moment of the high spin molecule in section IV. The next section concerns with the Josephson supercurrent plots. We bring out the fact that the $0-\pi$ junction behavior can be tuned via the spin of the high spin molecule. Section VI deals with the free energy of our system and we especially concentrate on the parameters necessary to exhibit bistable junction behavior, unnecessary precursor to Josephson qubits. The effects of interface transparency on the $0-\pi$ junction behavior is brought out in section VII. The exchange interactions between the High spin molecule and the electrons in normal metal can also play a crucial role on the tunability of $0-\pi$ Josephson junction, this is explored in section VIII. We reveal that the electron-electron interactions in our system has a insignificant role in the tunability of our π junction in section IX. Section X deals with the effect of the high spin molecule spin states on the Josephson supercurrent. These in contrast to electron-electron interactions have a nontrivial role in the tunability of our Josephson π junction. Finally, the paper ends with a perspective on future endeavors.

II. THEORY

A. Hamiltonian

The Hamiltonian¹³ used to describe a HSM is given by-

$$H_{HSM} = -DS_z^2 - J_0 \vec{s} \cdot \vec{S} \quad (1)$$

The first term characterizes the axial anisotropy of the HSM, D is an uniaxial anisotropy constant and S_z is the z component of the spin of the HSM. The electrons in the normal metals interact with HSM via the exchange term $-J_0\vec{s}\cdot\vec{S}$, where J_0 being the strength of the exchange interaction, \vec{s} is the electronic spin and \vec{S} is the spin of the HSM. $J_0(= \frac{\hbar^2 k_F J}{m^*})$, with J being the relative magnitude of the exchange interaction which ranges from 0 – 3 in this work, m^* is the electronic mass and Fermi wavevector k_F is obtained from the Free energy E_F which is the largest energy scale in our system 1000Δ , Δ - the superconducting gap for a widely used s-wave superconductor like lead is 1 meV. Substituting the value of the Fermi wavevector so obtained in the formula for J_0 we get $J_0 = 0.778$ eV (if $J = 2$). The magnitude of D is $56 \mu\text{eV}$ (see Ref. 14), thus the second term of equation (1) is almost 14000 times larger than first. Therefore we only consider the second term of equation (1) to represent the Hamiltonian of the high spin molecule. Our system consists of two normal metals with a HSM sandwiched between two conventional s-wave singlet superconductors. The superconductors are isotropic, and we consider an effective 1D model as shown in Fig. 1, it depicts a HSM at $x = 0$ and two superconductors at $x < -a/2$ and $x > a/2$. There are normal metal regions in $-a/2 < x < 0$ and $0 < x < a/2$. The model Hamiltonian in Bogoliubov-de Gennes formalism of our system is a 4×4 matrix which is given below:

$$\begin{pmatrix} H\hat{I} & i\Delta\hat{\sigma}_y \\ -i\Delta^*\hat{\sigma}_y & -H\hat{I} \end{pmatrix} \Psi(x) = E\Psi(x), \quad (2)$$

$H = p^2/2m^* + V[\delta(x + a/2) + \delta(x - a/2)] - J_0\delta(x)\vec{s}\cdot\vec{S} - E_F$, here $p^2/2m^*$ is the kinetic energy of an electron with effective mass m^* , V is the strength of the δ potential at the interfaces between normal metal and superconductor, J_0 is the strength of exchange interaction between the electron with spin \vec{s} and a HSM with spin \vec{S} . Further, Ψ is a four-component spinor, $\hat{\sigma}$ is Pauli spin matrix and \hat{I} is 2×2 unit matrix, E_F being the Fermi energy. The superconducting gap parameters Δ for left and right superconductor, are assumed to have the same magnitude but different phases φ_L and φ_R and are given by $\Delta = \Delta_0[e^{i\varphi_L}\theta(-x - a/2) + e^{i\varphi_R}\theta(x - a/2)]$, $\theta(x)$ is the Heaviside step function, Δ_0 is temperature dependent gap parameter and it follows $\Delta_0 \rightarrow \Delta_0 \tanh(1.74\sqrt{(T_c/T - 1)})$, where T_c is the superconducting critical temperature¹⁵.

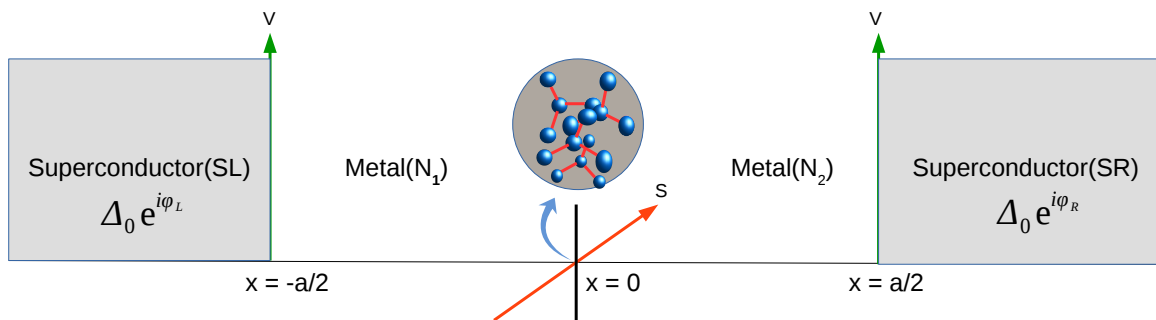


FIG. 1: Josephson junction composed of two normal metals and a high spin molecule with spin S and magnetic moment m' at $x = 0$ sandwiched between two s-wave superconductors.

B. Wavefunctions

There can be eight different types of quasiparticle injection into our system: an electron-like quasiparticle(ELQ) with spin up or down or a hole-like quasiparticle(HLQ) with spin up or down injected from either the left or from the right superconducting electrode. For the injection of spin up electron in left superconductor, the wave function is

given by¹⁶-

$$\psi_{SL}(x) = \begin{pmatrix} u \\ 0 \\ 0 \\ v \end{pmatrix} e^{iq_+x} \phi_{m'}^S + r_{ee}^{\uparrow\uparrow} \begin{pmatrix} u \\ 0 \\ 0 \\ v \end{pmatrix} e^{-iq_+x} \phi_{m'}^S + r_{ee}^{\uparrow\downarrow} \begin{pmatrix} 0 \\ u \\ -v \\ 0 \end{pmatrix} e^{-iq_+x} \phi_{m'+1}^S + r_{eh}^{\uparrow\uparrow} \begin{pmatrix} 0 \\ -v \\ u \\ 0 \end{pmatrix} e^{iq_-x} \phi_{m'+1}^S + r_{eh}^{\uparrow\downarrow} \begin{pmatrix} 0 \\ 0 \\ 0 \\ u \end{pmatrix} e^{iq_-x} \phi_{m'}^S, \quad \text{for } x < -\frac{a}{2}$$

The amplitudes $r_{ee}^{\uparrow\uparrow}, r_{ee}^{\uparrow\downarrow}, r_{eh}^{\uparrow\uparrow}, r_{eh}^{\uparrow\downarrow}$ represent normal reflection, normal reflection with spin flip, Andreev reflection with spin flip and Andreev reflection without flip respectively.

The corresponding wave function in the right superconductor is-

$$\psi_{SR}(x) = t_{ee}^{\uparrow\uparrow} \begin{pmatrix} ue^{i\varphi} \\ 0 \\ 0 \\ v \end{pmatrix} e^{iq_+x} \phi_{m'}^S + t_{ee}^{\uparrow\downarrow} \begin{pmatrix} 0 \\ ue^{i\varphi} \\ -v \\ 0 \end{pmatrix} e^{iq_+x} \phi_{m'+1}^S + t_{eh}^{\uparrow\uparrow} \begin{pmatrix} 0 \\ -ve^{i\varphi} \\ u \\ 0 \end{pmatrix} e^{-iq_-x} \phi_{m'+1}^S + t_{eh}^{\uparrow\downarrow} \begin{pmatrix} ve^{i\varphi} \\ 0 \\ 0 \\ u \end{pmatrix} e^{-iq_-x} \phi_{m'}^S, \quad \text{for } x > \frac{a}{2}$$

where $t_{ee}^{\uparrow\uparrow}, t_{ee}^{\uparrow\downarrow}, t_{eh}^{\uparrow\uparrow}, t_{eh}^{\uparrow\downarrow}$ are the transmission amplitudes, corresponding to the reflection process described above. $\phi_{m'}^S$ is the eigenspinor of the HSM, with its S^z operator acting as- $S^z \phi_{m'}^S = m' \phi_{m'}^S$, with m' being the spin magnetic

moment of the HSM. The BCS coherence factors are defined as $u = \sqrt{\frac{1}{2} \left(1 + \frac{\sqrt{E^2 - \Delta_0^2}}{E} \right)}$, $v = \sqrt{\frac{1}{2} \left(1 - \frac{\sqrt{E^2 - \Delta_0^2}}{E} \right)}$.

$q_{\pm} = \sqrt{\frac{2m^*}{\hbar^2} (E_F \pm \sqrt{E^2 - \Delta_0^2})}$ is the wavevector for electron-like quasiparticle(q_+) and hole-like quasiparticle(q_-) in the left and right superconducting wavefunctions, ψ_{SL} and ψ_{SR} . The wavefunction in the normal metal region(N_1) is given by-

$$\begin{aligned} \psi_{N_1}(x) = & (e e^{ik_e(x+a/2)} + f e^{-ik_e x}) \begin{pmatrix} 1 \\ 0 \\ 0 \\ 0 \end{pmatrix} \phi_{m'}^S + (e' e^{ik_e(x+a/2)} + f' e^{-ik_e x}) \begin{pmatrix} 0 \\ 1 \\ 0 \\ 0 \end{pmatrix} \phi_{m'+1}^S \\ & + (g e^{-ik_h(x+a/2)} + h e^{ik_h x}) \begin{pmatrix} 0 \\ 0 \\ 1 \\ 0 \end{pmatrix} \phi_{m'+1}^S + (g' e^{-ik_h(x+a/2)} + h' e^{ik_h x}) \begin{pmatrix} 0 \\ 0 \\ 0 \\ 1 \end{pmatrix} \phi_{m'}^S, \quad \text{for } -\frac{a}{2} < x < 0 \end{aligned}$$

Similarly the wavefunction in the normal metal region(N_2) is given by-

$$\begin{aligned} \psi_{N_2}(x) = & (a_0 e^{ik_e x} + b e^{-ik_e(x-a/2)}) \begin{pmatrix} 1 \\ 0 \\ 0 \\ 0 \end{pmatrix} \phi_{m'}^S + (a' e^{ik_e x} + b' e^{-ik_e(x-a/2)}) \begin{pmatrix} 0 \\ 1 \\ 0 \\ 0 \end{pmatrix} \phi_{m'+1}^S \\ & + (c e^{-ik_h x} + d e^{ik_h(x-a/2)}) \begin{pmatrix} 0 \\ 0 \\ 1 \\ 0 \end{pmatrix} \phi_{m'+1}^S + (c' e^{-ik_h x} + d' e^{ik_h(x-a/2)}) \begin{pmatrix} 0 \\ 0 \\ 0 \\ 1 \end{pmatrix} \phi_{m'}^S, \quad \text{for } 0 < x < \frac{a}{2} \end{aligned}$$

$k_{e,h} = \sqrt{\frac{2m^*}{\hbar^2} (E_F \pm E)}$ is the wave vector in the normal metals. In our work we have used the Andreev approximation¹² $q_+ = q_- = k_F$ and $k_{e,h} \approx k_F \pm \frac{k_F E}{2E_F}$, where k_F is the Fermi wavevector, with $E_F \gg \Delta$.

C. Boundary conditions

The boundary conditions at $x = -a/2$:

$$\psi_{SL}(x) = \psi_{N_1}(x), \quad (\text{continuity of wavefunctions}) \quad (3)$$

$$\frac{d\psi_{N_1}}{dx} - \frac{d\psi_{SL}}{dx} = \frac{2m^*V}{\hbar^2} \psi_{N_1}, \quad (\text{discontinuity in first derivative}) \quad (4)$$

and at $x = 0$:

$$\psi_{N_1}(x) = \psi_{N_2}(x) \quad (5)$$

$$\frac{d\psi_{N_2}}{dx} - \frac{d\psi_{N_1}}{dx} = -\frac{2m^*J_0\vec{s}\cdot\vec{S}}{\hbar^2}\psi_{N_1} \quad (6)$$

where $\vec{s}\cdot\vec{S}$ is the exchange operator in the Hamiltonian and is given by $\vec{s}\cdot\vec{S} = s^Z S^Z + \frac{1}{2}(s^- S^+ + s^+ S^-)$;

$$\vec{s}\cdot\vec{S} \begin{pmatrix} 1 \\ 0 \\ 0 \\ 0 \end{pmatrix} \phi_{m'}^S = mm' \begin{pmatrix} 1 \\ 0 \\ 0 \\ 0 \end{pmatrix} \phi_{m'}^S + \frac{1}{2}F_1 F_2 \begin{pmatrix} 0 \\ 1 \\ 0 \\ 0 \end{pmatrix} \phi_{m'+1}^S$$

and

$$\vec{s}\cdot\vec{S} \begin{pmatrix} 0 \\ 1 \\ 0 \\ 0 \end{pmatrix} \phi_{m'+1}^S = (m-1)(m'+1) \begin{pmatrix} 0 \\ 1 \\ 0 \\ 0 \end{pmatrix} \phi_{m'+1}^S + \frac{1}{2}F_1 F_2 \begin{pmatrix} 1 \\ 0 \\ 0 \\ 0 \end{pmatrix} \phi_{m'}^S$$

Here $F_1 = \sqrt{(s+m)(s-m+1)}$ is the spin-flip probability for electron and $F_2 = \sqrt{(S-m')(S+m'+1)}$ is the spin-flip probability¹⁷ for HSM. $s^\pm = s_x \pm is_y$ and $S^\pm = S_x \pm iS_y$ are the raising and lowering spin operators. Finally, at $x = a/2$:

$$\psi_{N_2}(x) = \psi_{SR}(x) \quad (7)$$

$$\frac{d\psi_{SR}}{dx} - \frac{d\psi_{N_2}}{dx} = \frac{2m^*V}{\hbar^2}\psi_{N_2}. \quad (8)$$

We will later use the dimensionless parameter $J = \frac{m^*J_0}{\hbar^2 k_F}$ as a measure of strength of exchange interaction and $Z = \frac{V}{V_0}$, with $V_0 = \frac{\hbar^2 k_F}{m^*}$ as a measure of interface transparency. Thus a value of $Z = 5$ (say) means interface potential $V = 5V_0$, with V in units of V_0 . By using above boundary conditions one can get the different scattering amplitudes. The wave functions for the other seven types of quasiparticle injection process are constructed in the same way.

III. JOSEPHSON CURRENT IN PRESENCE OF A HSM

A. Total Josephson current

Using the generalized version of the Furusaki-Tsukuda formalism¹⁸ we can calculate the total dc Josephson current-

$$I_T(\varphi) = \frac{e\Delta_0}{2\beta\hbar} \frac{1}{2\pi} \int_0^{2\pi} \sum_{\omega_n} \frac{q_+(\omega_n) + q_-(\omega_n)}{\Omega_n} \times \left[\frac{a_1(\omega_n) - a_2(\omega_n)}{q_+(\omega_n)} + \frac{a_3(\omega_n) - a_4(\omega_n)}{q_-(\omega_n)} \right] d(k_F a), \quad (9)$$

herein $\omega_n = (2n+1)\pi/\beta$ are fermionic Matsubara frequencies with $n = 0, \pm 1, \pm 2, \dots$ and $\Omega_n = \sqrt{\omega_n^2 + \Delta_0^2}$. $\beta = 1/kT$ is the inverse temperature. $q_+(\omega_n), q_-(\omega_n)$, and $a_i(\omega_n)$ are obtained from q_+, q_- and a_i by analytically continuing E to $i\omega_n$. Here $a_i (i = 1, 2, 3, 4)$ with $a_1 = r_{eh}^{\uparrow\downarrow}$ is the Andreev reflection coefficient without flip for electron up incident in left superconductor, similarly $a_2 = r_{eh}^{\downarrow\uparrow}$ is the Andreev reflection coefficient without flip for electron down incident in left superconductor, $a_3 = r_{he}^{\uparrow\downarrow}$ and $a_4 = r_{he}^{\downarrow\uparrow}$ are the Andreev reflection coefficients without flip for hole up and hole down incident in left superconductor respectively. We sum over the Matsubara frequencies numerically. The detailed balance conditions¹⁸ are verified as follows:

$$\frac{a_1(-\varphi, E)}{q_+} = \frac{a_4(\varphi, E)}{q_-}, \quad \frac{a_2(-\varphi, E)}{q_+} = \frac{a_3(\varphi, E)}{q_-}$$

B. Bound state contribution

Neglecting the contribution from incoming quasiparticle¹⁶ and inserting the wave function into the boundary conditions, we get a homogeneous system of 24 linear equations for the scattering amplitudes. If we express the scattering amplitudes in the two normal metal regions by the scattering amplitudes in the left and right superconductor we get a homogeneous system of 8 linear equations¹⁵,

$$Mx = 0 \quad (10)$$

where x is a 8×1 column matrix and is given by $x = [r_{ee}^{\uparrow\uparrow}, r_{ee}^{\uparrow\downarrow}, r_{eh}^{\uparrow\uparrow}, r_{eh}^{\uparrow\downarrow}, t_{ee}^{\uparrow\uparrow}, t_{ee}^{\uparrow\downarrow}, t_{eh}^{\uparrow\uparrow}, t_{eh}^{\uparrow\downarrow}]$ and M is a 8×8 matrix which is explicitly written in Appendix A. For a nontrivial solution of this system of equations, $\det M = 0$, we can get a relation between the Andreev bound state energy and phase difference, i.e., Andreev levels with dispersion E_i , $i = \{1, \dots, 4\}$ ¹⁹. We find that $E_i(\varphi) = E_\sigma^\pm(\varphi) = \pm E_\sigma(\varphi)$, ($\sigma = \uparrow, \downarrow$) and

$$E_\sigma^\pm(\varphi) = \pm \Delta_0 \sqrt{\frac{|A(\varphi)| + \rho_\sigma \sqrt{|B(\varphi)|}}{2|C|}} \quad (11)$$

wherein $\rho_{\uparrow(\downarrow)} = +1(-1)$ and $A(\varphi), B(\varphi), C$ depend on all junction parameters. Their explicit form is given in Appendix B. For simplicity we have taken all wavevectors equal to the Fermi wavevector (Andreev approximation). For transparent regime ($Z = 0$) we find-

$$\begin{aligned} E_\sigma^\pm(\varphi) = & \pm \frac{\Delta_0}{\sqrt{2}} (\sqrt{((2(8 + J^4(F_2^2 + m' + m'^2)^2 + J^2(3 + 2F_2^2 + 6m'(1 + m')) + (8 + J^2(1 - 2F_2^2 + 2m'(1 + m')))) \cos(\varphi))} \\ & + \rho_\sigma \sqrt{(2J^2(64F_2^4 J^2 + 3(J + 2Jm')^2 + 4F_2^2(16 + J^2(5 + 4m'(1 + m')))) + 4J^2(-4F_2^2 + 16F_2^4 - (1 + 2m')^2) \cos(\varphi))} \\ & + ((J + 2Jm')^2 - 4F_2^2(16 + (J + 2Jm')^2)) \cos(2\varphi)) / (16 + J^4(F_2^2 + m' + m'^2)^2 + J^2(4 + 8F_2^2 + 8m'(1 + m')))) \end{aligned} \quad (12)$$

For $Z = 0$, interestingly the bound states are independent of any phase ($k_F a$) accumulated in normal metal region. For tunneling regime ($Z \rightarrow \text{Large}$) we get-

$$E_\sigma^\pm(\varphi) = \pm \Delta_0 \left[1 + \frac{(8 + J^2(1 - 2F_2^2 + 2m'(1 + m')) + (8 + J^2(-1 + 2F_2^2 - 2m'(1 + m')))) \cos(k_F a) \cos(\varphi)}{16Z^4 \sin(\frac{k_F a}{2})^2 (4 - J^2(F_2^2 + m' + m'^2) + (4 + J^2(F_2^2 + m' + m'^2)) \cos(k_F a) + 2J \sin(k_F a))^2} \right] \quad (13)$$

For $Z \rightarrow \text{Large}$, we can clearly say that bound states are phase ($k_F a$) dependent. From Andreev bound states energies Eq. 11 we can derive the Josephson bound state current²⁰-

$$I_B(\varphi) = \frac{2e}{\hbar} \frac{1}{2\pi} \int_0^{2\pi} \sum_i f(E_i) \frac{dE_i}{d\varphi} d(k_F a) = -\frac{2e}{\hbar} \frac{1}{2\pi} \int_0^{2\pi} \sum_\sigma \tanh\left(\frac{\beta E_\sigma}{2}\right) \frac{dE_\sigma}{d\varphi} d(k_F a) \quad (14)$$

wherein e is the electronic charge and $f(E_i)$ denotes the Fermi-Dirac distribution function. For transparent regime ($Z = 0$) we obtain the current-phase relation

$$\begin{aligned} \frac{I_B(\varphi)}{I_0} = & \Delta_0 \sin(\varphi) \left(\frac{1}{E_\uparrow} (\sqrt{2} J^4 (-4F_2^2 + 16F_2^4 - (1 + 2m')^2) + 8\sqrt{(J^2(64F_2^4 J^2 + 3(J + 2Jm')^2 + 4F_2^2(16 + J^2(5 \right. \\ & + 4m'(1 + m')) + 4J^2(-4F_2^2 + 16F_2^4 - (1 + 2m')^2) \cos(\varphi) + ((J + 2Jm')^2 - 4F_2^2(16 + (J + 2Jm')^2)) \cos(2\varphi))} \\ & + J^2(\sqrt{2}((J + 2Jm')^2 - 4F_2^2(16 + (J + 2Jm')^2)) \cos(\varphi) + (1 - 2F_2^2 + 2m'(1 + m')) \sqrt{(J^2(64F_2^4 J^2 + 3(J + 2Jm')^2} \\ & + 4F_2^2(16 + J^2(5 + 4m'(1 + m')) + 4J^2(-4F_2^2 + 16F_2^4 - (1 + 2m')^2) \cos(\varphi) + ((J + 2Jm')^2 - 4F_2^2(16 \\ & + (J + 2Jm')^2)) \cos(2\varphi))} \tanh\left(\frac{\beta E_\uparrow}{2}\right) + \frac{1}{E_\downarrow} (\sqrt{2} J^4 (4F_2^2 - 16F_2^4 + (1 + 2m')^2) + 8\sqrt{(J^2(64F_2^4 J^2 + 3(J + 2Jm')^2} \\ & + 4F_2^2(16 + J^2(5 + 4m'(1 + m')) + 4J^2(-4F_2^2 + 16F_2^4 - (1 + 2m')^2) \cos(\varphi) + ((J + 2Jm')^2 - 4F_2^2(16 \\ & + (J + 2Jm')^2)) \cos(2\varphi))} + J^2(\sqrt{2}(64F_2^2 + (-1 + 4F_2^2)(J + 2Jm')^2) \cos(\varphi) + (1 - 2F_2^2 + 2m'(1 + m')) \\ & \sqrt{(J^2(64F_2^4 J^2 + 3(J + 2Jm')^2 + 4F_2^2(16 + J^2(5 + 4m'(1 + m')) + 4J^2(-4F_2^2 + 16F_2^4 - (1 + 2m')^2) \cos(\varphi) \\ & + ((J + 2Jm')^2 - 4F_2^2(16 + (J + 2Jm')^2)) \cos(2\varphi))} \tanh\left(\frac{\beta E_\downarrow}{2}\right) / ((16 + J^4(F_2^2 + m' + m'^2)^2 + J^2(4 + 8F_2^2 \\ & + 8m'(1 + m')) \sqrt{(J^2(64F_2^4 J^2 + 3(J + 2Jm')^2 + 4F_2^2(16 + J^2(5 + 4m'(1 + m')) + 4J^2(-4F_2^2 + 16F_2^4 \\ & - (1 + 2m')^2) \cos(\varphi) + ((J + 2Jm')^2 - 4F_2^2(16 + (J + 2Jm')^2)) \cos(2\varphi))} \end{aligned} \quad (15)$$

where $I_0 = e\Delta_0/\hbar$ and $E_{\uparrow(\downarrow)}$ is given in equation 12. For tunneling regime ($Z \rightarrow \text{Large}$) and at $T = 0$ we find

$$\frac{I_B(\varphi)}{I_0} = \frac{1}{2\pi} \int_0^{2\pi} \left[\frac{(8 + J^2(1 - 2F_2^2 + 2m'(1 + m'))) + (8 + J^2(-1 + 2F_2^2 - 2m'(1 + m')))\cos(k_F a)\sin(\varphi)}{4Z^4 \sin(\frac{k_F a}{2})^2(4 - J^2(F_2^2 + m' + m'^2)) + (4 + J^2(F_2^2 + m' + m'^2))\cos(k_F a) + 2J \sin(k_F a)^2} \right] d(k_F a) \quad (16)$$

C. Continuum contribution

The continuum contribution to the Josephson current is the collection of currents carried by both electronlike and holelike quasiparticles outside the gap. Using the formalisms developed earlier in references 11, 21 the continuum contribution from electronlike excitations is given below.¹¹

$$I_C^e(\varphi) = \frac{2e}{h} \frac{1}{2\pi} \int_0^{2\pi} \left(\int_{-\infty}^{-\Delta_0} + \int_{\infty}^{\Delta_0} \right) \frac{1}{|u^2 - v^2|} \times [T_{L \rightarrow R}^{e\uparrow\uparrow}(E, \varphi) + T_{L \rightarrow R}^{e\uparrow\downarrow}(E, \varphi) - T_{L \leftarrow R}^{e\uparrow\uparrow}(E, \varphi) - T_{L \leftarrow R}^{e\uparrow\downarrow}(E, \varphi)] f(E) dE d(k_F a) \quad (17)$$

Similarly the continuum contribution from holelike excitations can be calculated by replacing 'e' in Eq. 17 by 'h'. In Eq. 17 $T_{L \rightarrow R}^{e\uparrow\uparrow} = |t_{ee}^{\uparrow\uparrow}|^2 - |t_{eh}^{\uparrow\uparrow}|^2$ is the transmission without flip for the electronic currents moving from left to right of the system as depicted in Fig. 1. $T_{L \rightarrow R}^{e\uparrow\downarrow} = |t_{ee}^{\uparrow\downarrow}|^2 - |t_{eh}^{\uparrow\downarrow}|^2$ is the transmission with flip for the electronic currents moving from left to right of the system and similarly $T_{L \leftarrow R}^{e\uparrow\uparrow}$ and $T_{L \leftarrow R}^{e\uparrow\downarrow}$ are the transmission without flip and with flip for the electronic currents moving from right to left of the system respectively. Here we have

$$T_{L \leftarrow R}^{e\uparrow\uparrow}(E, \varphi) = T_{L \rightarrow R}^{e\uparrow\uparrow}(E, -\varphi), T_{L \leftarrow R}^{e\uparrow\downarrow}(E, \varphi) = T_{L \rightarrow R}^{e\uparrow\downarrow}(E, -\varphi)$$

The hole continuum contribution is found to be equal to the electronic continuum contribution. Therefore, the total continuum current due to electron-like and hole-like excitations is given as follows:

$$I_C(\varphi) = \frac{I_C^e(\varphi) + I_C^h(\varphi)}{2} = I_C^e(\varphi) \quad (18)$$

In our work we have verified the total current conservation- $I_T(\varphi) = I_B(\varphi) + I_C(\varphi)$

IV. ANDREEV BOUND STATES

The Andreev bound states (ABS) as obtained in Eq. 11 are analyzed in this section. We focus on the role of spin S and magnetic moment m' of the HSM on ABS. In Fig. 2(a), we plot ABS for $S = 1/2$ and $m' = 1/2$, as here the spin flip probability $F_2 = \sqrt{(S - m')(S + m' + 1)} = 0$ which corresponds to no flip, we get only two bound states, but in Fig. 2(b) with $S = 1/2$ and $m' = -1/2$, $F_2 \neq 0$ thus due to spin flip processes we get four bound states. To address the situation of large spin S in HSM in Fig. 3 we plot ABS for $S = 9/2$ and all allowed m' values. For particular S , as

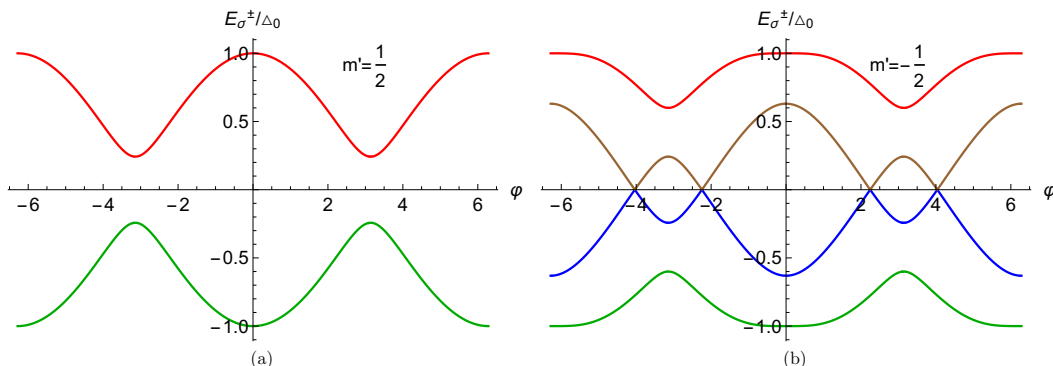


FIG. 2: Andreev bound states as a function of phase difference (φ). Parameters are $\Delta_0 = 1\text{meV}$, $S = 1/2$, $m' = \pm 1/2$, $J = 1$, $Z = 0$.

m' changes, separation between electron (positive) bound states and hole (negative) bound states increases. Similarly for particular m' as we change S , this separation increases. For large S , ABS lie at the gap edge. This is seen for large m' as well. This behavior is also seen as one changes J , Z as well. We only plot ABS for $m' = \pm 1/2, \pm 3/2, \pm 9/2$, but we do not plot for $m' = \pm 5/2, \pm 7/2$ because the separation between electron bound states and hole bound states increases from $m' = 3/2$ to $m' = 9/2$ and these m' values lie between $m' = 3/2$ and $m' = 9/2$. Large S , m' , Z , J lead to ABS shifting to gap edge.

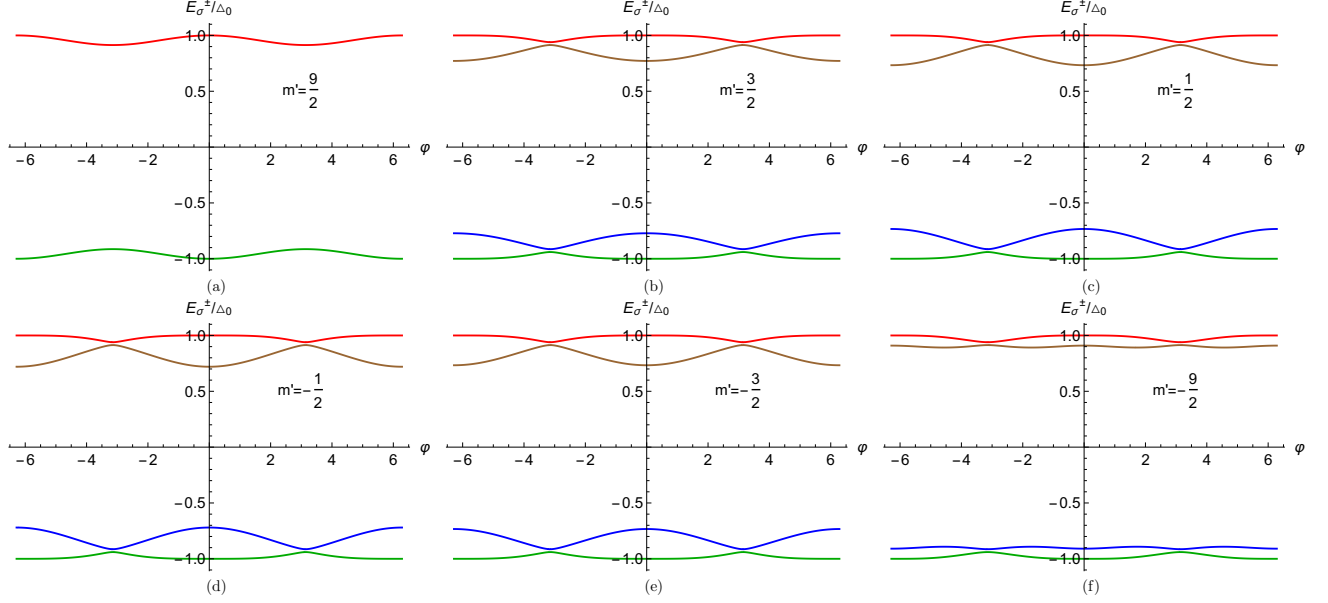


FIG. 3: Andreev bound states as a function of phase difference (φ). Parameters are $\Delta_0 = 1\text{meV}$, $S = 9/2$, $m' = \pm 1/2, \pm 3/2, \pm 9/2$, $J = 1$, $Z = 0$.

V. JOSEPHSON CURRENT: π JUNCTION

The considered model shows π junction behavior. To see this, we plot the bound state, continuum and total Josephson currents for $S = 1/2$ (Fig. 4) and $S = 9/2$ (Fig. 5). We choose the transparent regime ($Z = 0$) case. A separate section will be devoted to effect of tunnel contacts. One can clearly conclude that the continuum contribution of the total current is very small, therefore the bound current and total current are almost same. In Fig. 4(a) as there is no flip we have 0 junction. For spin flip case, the Josephson current changes sign in $0 < \varphi < \pi$ regime. In Fig. 5

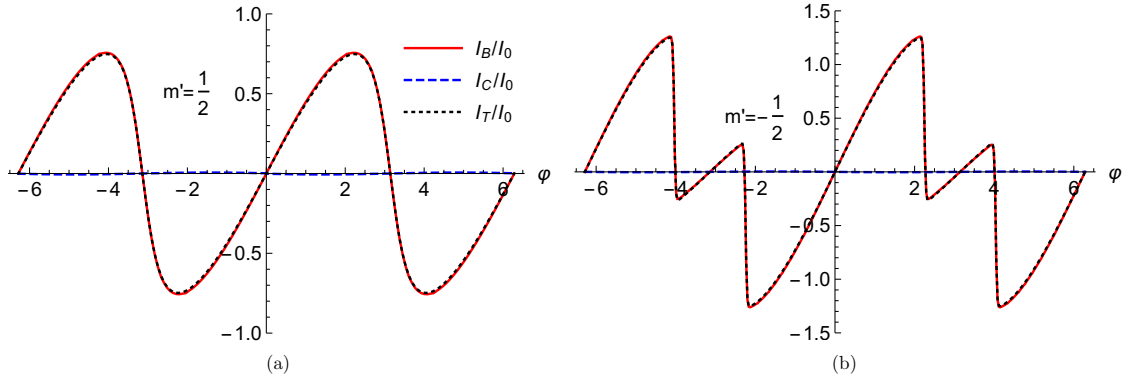


FIG. 4: The bound, continuum and total Josephson current as a function of phase difference (φ). Parameters are $\Delta_0 = 1\text{meV}$, $T/T_c = 0.01$, $S = 1/2$, $m' = \pm 1/2$, $J = 1$, $Z = 0$.

we concentrate on high spin ($S = 9/2$) of HSM. Here we also see that for $m' = 5/2, 3/2, 1/2, -1/2, -3/2, -5/2, -7/2$ we get π junction. But for $m' = 9/2, 7/2, -9/2$ we get 0 junction. So here also there will be a switching from 0 to π and again from π to 0 with change of m' from $9/2$ to $-9/2$. Thus, one can conclude that all π shifts are due to spin flip scattering ($F_2 \neq 0$), however the reverse is not necessarily true.

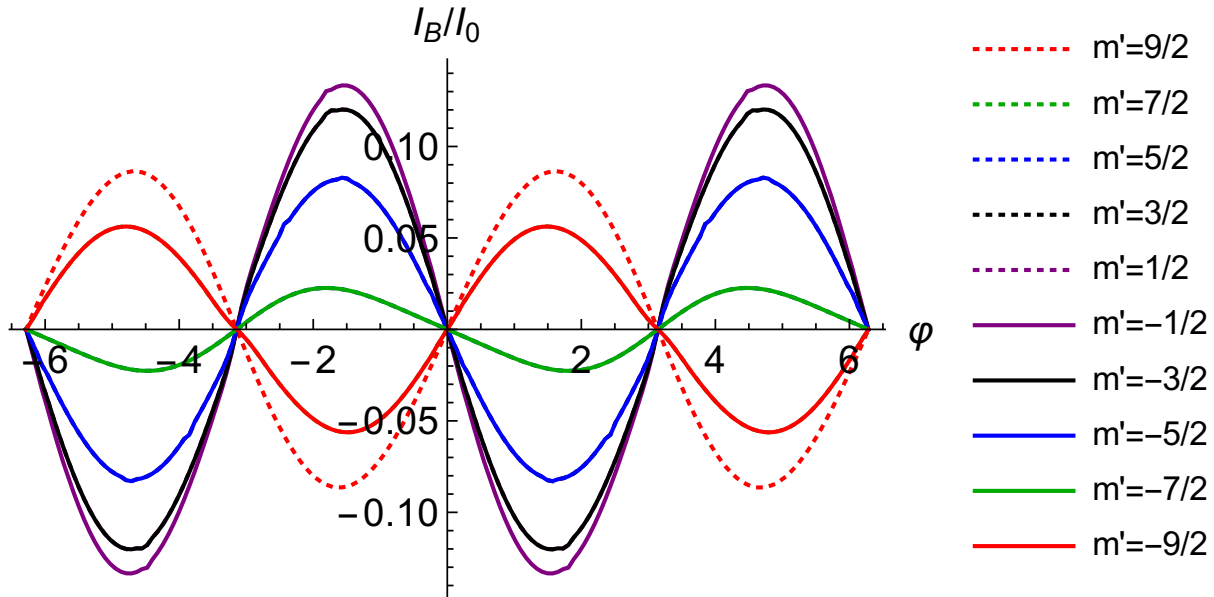


FIG. 5: Josephson supercurrent as a function of phase difference (φ). Parameters are $\Delta_0 = 1\text{meV}$, $T/T_c = 0.01$, $S = 9/2$, $m' = \pm 9/2, \pm 7/2, \pm 5/2, \pm 3/2, \pm 1/2$, $J = 1$, $Z = 0$. Josephson supercurrent for $m' = 7/2$ and $m' = -9/2$ are same and similarly for $m' = 5/2$ and $m' = -7/2$, $m' = 3/2$ and $m' = -5/2$, $m' = 1/2$ and $m' = -3/2$ are same.

VI. FREE ENERGY

We can also determine the nature of the junction, i.e. 0 or π by the minimum of the free energy, which is given by

$$F(\varphi) = -\frac{1}{\beta} \frac{1}{2\pi} \int_0^{2\pi} \ln \left[\prod_i (1 + e^{-\beta E_i(\varphi)}) \right] d(k_F a) = -\frac{2}{\beta} \frac{1}{2\pi} \int_0^{2\pi} \sum_{\sigma} \ln \left[2 \cosh \left(\frac{\beta E_{\sigma}(\varphi)}{2} \right) \right] d(k_F a) \quad (19)$$

In Fig. 6 we have plotted F/Δ_0 as a function of phase difference for spin $S = 9/2$ and different values of m' , we have considered a transparent junction ($Z = 0$). In the same figure we see that the free energy for $m' = 9/2$ is almost half than that of the other cases ($m' \neq 9/2$). A plausible reason for why these occurs could be that for $m' = 9/2$ there is no spin flip process ($F_2 = 0$) while for the other cases F_2 ranges from 3 to 5. In Fig. 7 we plot the Free energy for $S = 5/2$ and $m' = 1/2$ for different values of interface transparency Z . At particular value of $Z = 0.383$ the Free energy shows a bistable behavior, i.e., the Free energy minima occurs at both 0 and π meaning that the ground state of the system does not occur at either 0 or π exclusively but is shared by both. These bistable junctions have a major role to play in quantum computation applications²²⁻²⁴.

VII. EFFECT OF TUNNEL CONTACTS

In Fig. 8 we plot the Josephson supercurrent as a function of phase difference for different values of interface barrier strength. From Fig. 8(a) where $m' = 5/2$ we see that there is no π shift from transparent to tunnel regime and the ground state of the system always stays at $\varphi = 0$. The reason that ground state stays at $\varphi = 0$ in Fig. 8(a) is because of the absence of spin flip processes as $S = m' = 5/2$ and $F_2 = 0$. In Fig. 8(b) the ground state of the system shifts from $\varphi = \pi$ to $\varphi = 0$ as a function of Z . Infact for a transparent junction ($Z = 0$) the ground state is at $\varphi = \pi$ and as we increase Z we see the ground state shift from π to 0 state. Of course in this case as $S = 5/2$ and $m' = 1/2$ therefore the probability for the HSM to flip ($F_2 \neq 0$) is nonzero. Thus spin flip processes aid in the transition from

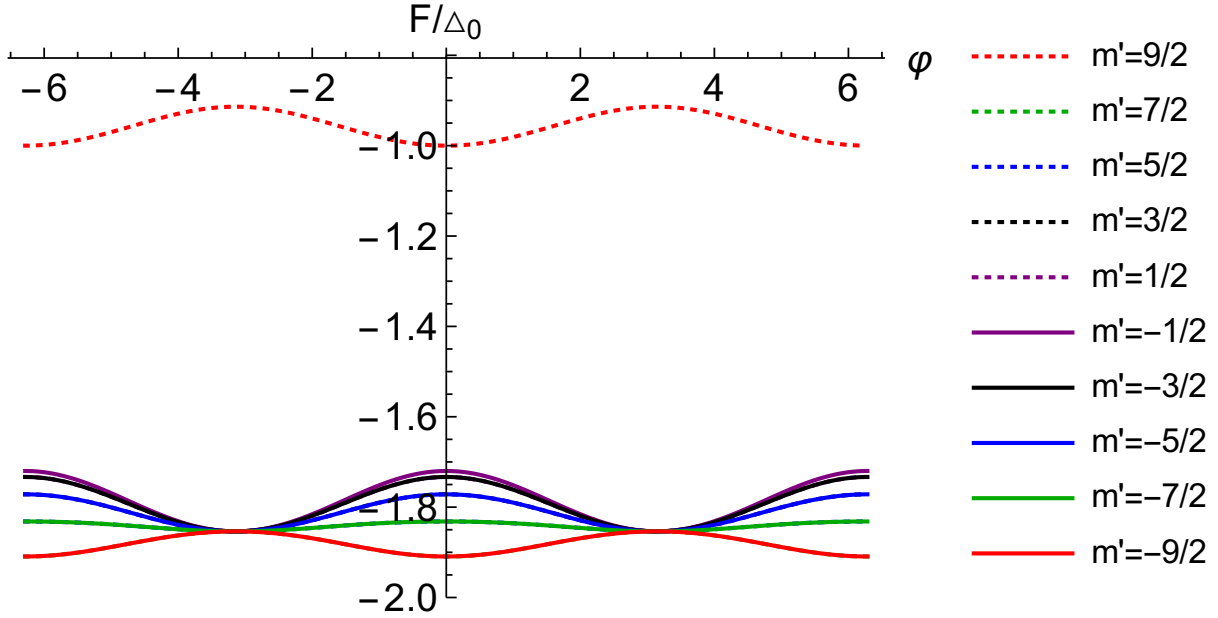


FIG. 6: Free energy as a function of phase difference (φ). Parameters are $\Delta_0 = 1\text{meV}$, $T/T_c = 0.01$, $S = 9/2$, $m' = \pm 9/2, \pm 7/2, \pm 5/2, \pm 3/2, \pm 1/2$, $J = 1$, $Z = 0$. Free energy for $m' = 7/2$ and $m' = -9/2$ are same and similarly for $m' = 5/2$ and $m' = -7/2$, $m' = 3/2$ and $m' = -5/2$, $m' = 1/2$ and $m' = -3/2$ are same.

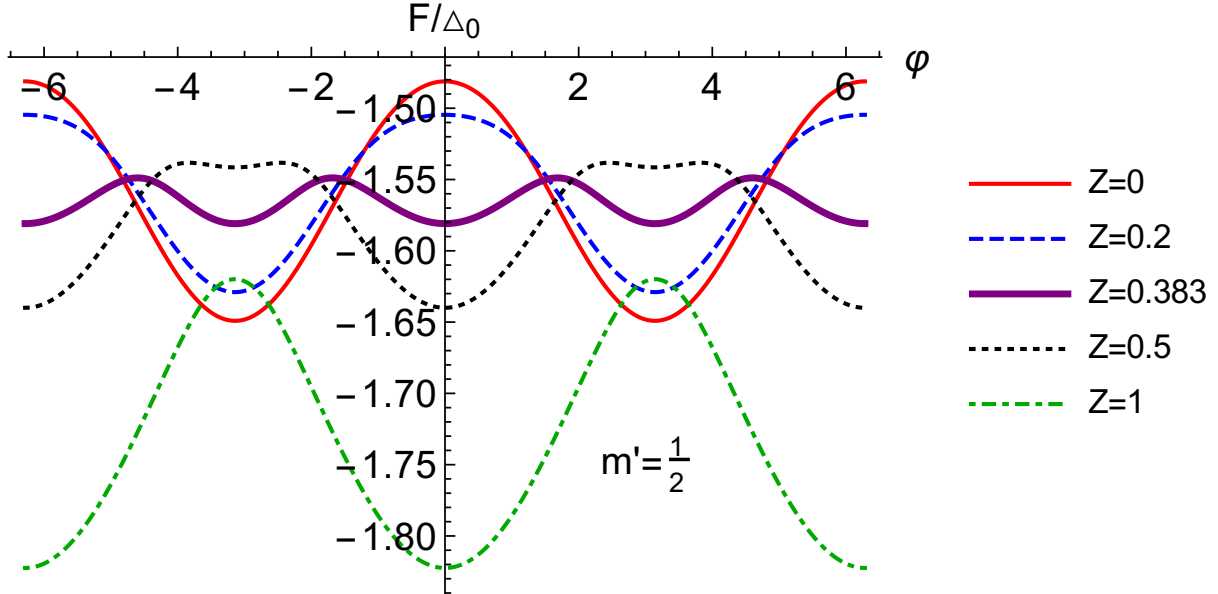


FIG. 7: Free energy as a function of phase difference (φ) for different values of interface barrier strength (Z). Parameters are $\Delta_0 = 1\text{meV}$, $T/T_c = 0.01$, $S = 5/2$, $m' = 1/2$, $J = 1$.

0 to π junction. Notably, this transition can be tuned by the transparency of the junction (Z) as is evident from Fig. 8(b). Of course not all cases where in the HSM flips its spin leads to a transition from 0 to π state as is evident in Fig. 8(c). In Fig. 8(c) the ground state stays at $\varphi = 0$, but here as $S = 5/2$, $m' = 3/2$ and $F_2 \neq 0$, so spin flip processes occur in contrast to Fig. 8(a). In Fig. 8 the strength of exchange interaction J is taken as 1. It has to be pointed out that J has a nontrivial role in the 0 to π state transition as will be evident in the next section. Thus are conclusions regarding Fig. 8(c) has to be qualified by the fact that we haven't focused on the issue of exchange interaction so far.

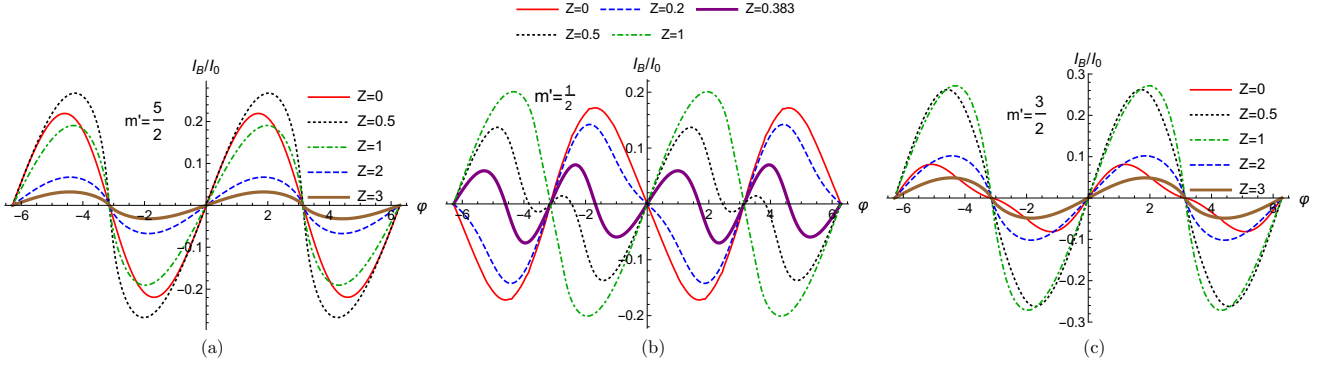


FIG. 8: Josephson supercurrent as a function of phase difference (φ) for different values of interface barrier strength (Z). Parameters are $\Delta_0 = 1\text{meV}$, $T/T_c = 0.01$, $J = 1$, $S = 5/2$ and for (a) $m' = 5/2$, (b) $m' = 1/2$ and (c) $m' = 3/2$. Josephson supercurrent for $m' = 3/2$ and $m' = -5/2$ are same and similarly $m' = 1/2$ and $m' = -3/2$ are same.

VIII. EFFECT OF EXCHANGE COUPLING

In Hamiltonian H , in Eq. (2) the term $J_0\delta(x)\vec{s}\cdot\vec{S}$ represents the exchange coupling of strength J_0 between the electron with spin \vec{s} and a HSM with spin \vec{S} . In Fig. 9 the Josephson supercurrent is plotted as a function of phase difference for different values of strength of exchange interaction in the transparent regime. We choose $S = 5/2$ and allowed values of m' . One sees for the no spin flip case there is no transition from 0 to π junction while for cases with spin flip one can see a 0 to π state transition. Thus all spin flip process i.e., $F_2 \neq 0$ and with $J > 2$ show π junction behavior.

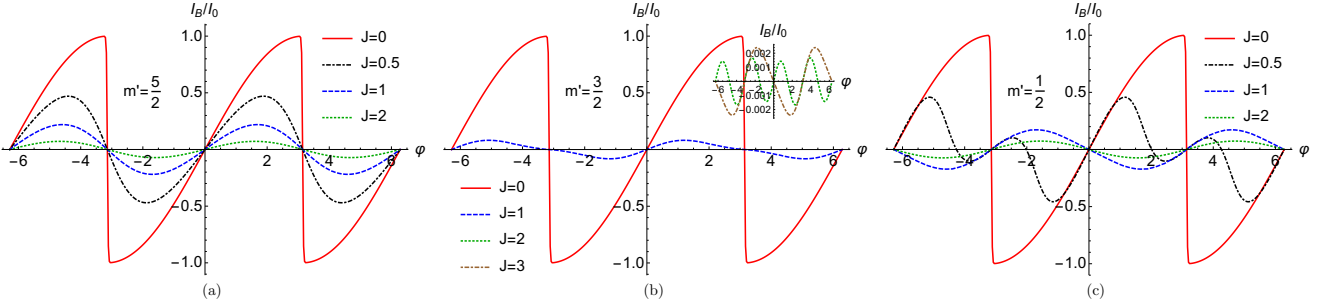


FIG. 9: Josephson supercurrent as a function of phase difference (φ) for different values of exchange interaction (J). Parameters are $\Delta_0 = 1\text{meV}$, $T/T_c = 0.01$, $Z = 0$, $S = 5/2$ for (a) $m' = 5/2$, (b) $m' = 3/2$ and (c) $m' = 1/2$. Josephson supercurrent for $m' = 3/2$ and $m' = -5/2$ are same and similarly $m' = 1/2$ and $m' = -3/2$ are same.

IX. EFFECT OF ELECTRON-ELECTRON INTERACTION (PHENOMENOLOGICAL):

We have considered a phenomenological^{25,26} approach to electron-electron interactions. The effect of such interactions are included through an energy dependent transmission probability which is given as-

$$T(E) = \frac{T_0 \left| \frac{E}{D_0} \right|^\alpha}{1 - T_0 \left(1 - \left| \frac{E}{D_0} \right|^\alpha \right)} \quad (20)$$

with T_0 being the transparency of the metal superconductor interface in the absence of electron-electron interactions. α ($0 < \alpha < 1$) represents the electron-electron interaction strength ($\alpha = 0$ corresponds to no interactions while $\alpha = 1$ corresponds to a maximally interacting system), D_0 is a high energy cutoff obtained by the energy bandwidth of

the electronic states. Now for non-interacting case the parameter Z is a constant and is related to the transmission probability T_0 as

$$Z^2 = \frac{1 - T_0}{T_0} \quad (21)$$

Now in presence of electron-electron interaction, T_0 is replaced by $T(E)$ in the above equation. Thus, the interface transparency Z which is considered identical at both interfaces will be energy dependent and will change from Z to Z_{ee} :

$$Z_{ee}^2 = \left| \frac{E}{D_0} \right|^{-\alpha} \frac{1 - T_0}{T_0} = \left| \frac{E}{D_0} \right|^{-\alpha} Z^2 \quad (22)$$

For $Z = 0$ ($T_0 = 1$), $Z_{ee} = 0$ which implies that for a transparent interface electron-electron interaction have no effect on electronic transport. In Fig. 10 we plot the Josephson supercurrent as a function of phase difference for different values of electron-electron interaction parameter α . We see that for $m' = 5/2, 1/2, -3/2$ there is no $0-\pi$ transition with increase of electron-electron interaction strength. But for $m' = 3/2, -1/2, -5/2$ there will be a tuning from π junction to 0 junction with increase of electron-electron interaction strength.

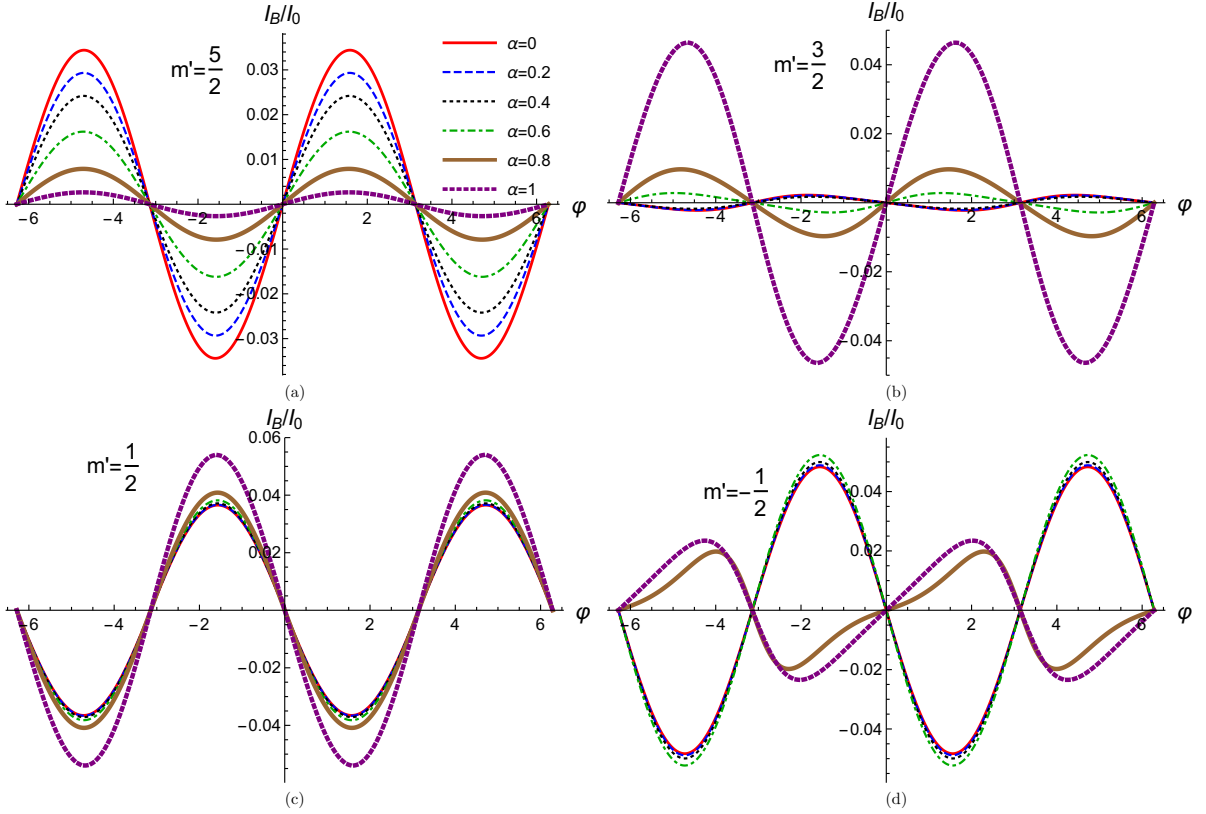


FIG. 10: Josephson supercurrent as a function of phase difference for different values of electron-electron interaction strength. Parameters are $\Delta_0 = 1\text{meV}$, $D_0 = 100\Delta_0$, $T/T_c = 0.01$, $J = 3$, $Z = 0.1$, $S = 5/2$ and for (a) $m' = 5/2$, (b) $m' = 3/2$, (c) $m' = 1/2$ and (d) $m' = -1/2$. Josephson supercurrent for $m' = 3/2$ and $m' = -5/2$ are same and similarly $m' = 1/2$ and $m' = -3/2$ are same.

X. EFFECT OF HIGH SPIN/MAGNETIC MOMENT STATES

Since we have a high spin molecule it is imperative for us to study high spin states of our HSM. In Fig. 11(a) we see that Josephson supercurrent at $\varphi = \pi/2$ is positive for $S = 1/2$, but as we increase spin(S) of HSM it changes to negative from $S = 3/2$ to $S = 9/2$. We choose phase difference $\varphi = \pi/2$ because at $\varphi = \pi/2$ we get maximum

Josephson supercurrent. In the inset of Fig. 11(a) we plot the Josephson supercurrent for still higher spin states of HSM ($S = 11/2 - 19/2$). In Fig. 11(a) for all different values of S the magnetic moment of HSM $m' = -1/2$ and the junction transparency $Z = 0$. The reason for the change in sign in the Josephson supercurrent can be guessed from the fact that the spin flip probability (F_2) of the HSM for negative Josephson supercurrent is greater than 1. This previous statement is however subject to qualification-negative supercurrent for low spin states of HSM require smaller values of spin flip probability F_2 than do high spin states of HSM. In Fig. 11(b) we look at the effect of spin magnetic moment states on Josephson supercurrent. We consider the spin S of HSM to be $9/2$. The Josephson supercurrent changes sign with m' . One can clearly see when the spin flip probability of HSM i.e., $F_2 > 3$ the Josephson supercurrent is negative but for flip probability $F_2 < 3$ the Josephson supercurrent is positive for a transparent junction $Z = 0$. We see in Fig. 11(c) the possibility of a π junction also at $Z = 1$ (intermediate transparency). In Fig. 11(c) we plot the Josephson supercurrent including still higher spin states of HSM ($S = 1/2 - 19/2$). In Appendix C we juxtapose the spin state S , magnetic moment m' and spin flip probability F_2 of HSM in a tabular format. Finally in Fig. 11(d) we plot the Josephson supercurrent at $Z = 1$ (non transparent junction) as a function of spin magnetic moment m' for $S = 9/2$. We see non transparent junction inhibit a $0 - \pi$ junction transition for $S = 9/2$. However, one has to qualify the aforesaid statement by looking at Fig. 11(c). In Fig. 11(c) we see that a finite Z (equal 1) can act as a barrier to the $0 - \pi$ junction transition. To overcome this barrier one needs to go to still higher spin states like $S = 15/2 - 19/2$. Thus in Fig. 11(d) instead of plotting for $S = 9/2$ if we had plotted for $S = 15/2 - 19/2$ we would have seen a $0 - \pi$ junction transition for some value of m' . So to conclude this section for transparent interfaces spin flip processes lead to a 0 to π junction transition. However, when junction transparency reduces one has to go to much higher spin states to see a $0 - \pi$ junction transition. The moral of the story is a finite Z inhibits $0 - \pi$ transition but a large S can overcome the Z barrier.

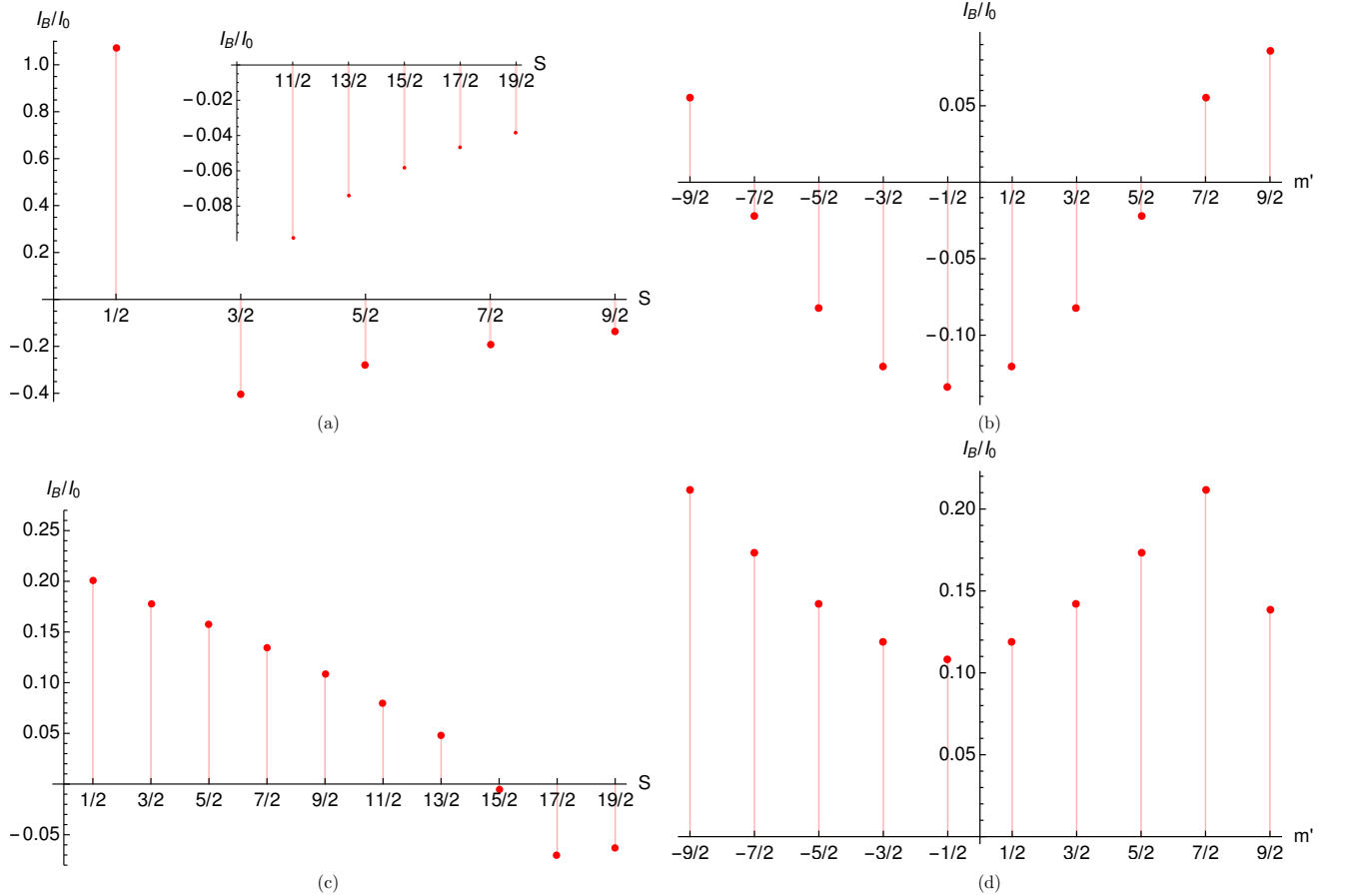


FIG. 11: (a) Josephson supercurrent vs HSM spin (S). Parameters are $\Delta_0 = 1\text{meV}$, $T/T_c = 0.01$, $\varphi = \pi/2$, $J = 1$, $m' = -1/2$, $Z = 0$, (b) Josephson supercurrent vs HSM magnetic moment (m'). Parameters are $\Delta_0 = 1\text{meV}$, $T/T_c = 0.01$, $\varphi = \pi/2$, $J = 1$, $S = 9/2$, $Z = 0$, (c) Josephson supercurrent vs HSM spin (S). Parameters are $\Delta_0 = 1\text{meV}$, $T/T_c = 0.01$, $\varphi = \pi/2$, $J = 1$, $m' = -1/2$, $Z = 1$, (d) Josephson supercurrent vs HSM magnetic moment (m'). Parameters are $\Delta_0 = 1\text{meV}$, $T/T_c = 0.01$, $\varphi = \pi/2$, $J = 1$, $S = 9/2$, $Z = 1$.

XI. CONCLUSIONS

In this paper we have provided an exhaustive study of the nature of the 0 to π Josephson junction transition in presence of a high spin molecule. We have studied various aspects of the problem like the strength of the exchange interaction (J) between HSM and charge carriers (Section VIII), the effect of electron-electron interactions (α) albeit phenomenologically (Section IX), effect of junction transparencies (Z) (Section VII) and of course the high spin states S , spin magnetic moment m' of the HSM itself (Section X). We identify spin flip probability of the HSM as the key to understand the 0 to π junction transition. We also focused on applications of our junction in quantum computation proposals (Section VI). This work will thus help experimentalist in designing π junctions without taking recourse to Ferromagnets or high T_c superconductors but with only a high spin molecule.

ACKNOWLEDGMENTS

This work was supported by the grant ‘‘Non-local correlations in nanoscale systems: Role of decoherence, interactions, disorder and pairing symmetry’’ from SCIENCE & ENGINEERING RESEARCH BOARD, New Delhi, Government of India, Grant No. EMR/2015/001836, Principal Investigator: Dr. Colin Benjamin, National Institute of Science Education and Research, Bhubaneswar, India.

APPENDIX A: EXPLICIT FORM OF MATRIX M

$$M = \begin{pmatrix} M_{11} & M_{12} & M_{13} & M_{14} & M_{15} & M_{16} & M_{17} & M_{18} \\ M_{21} & M_{22} & M_{23} & M_{24} & M_{25} & M_{26} & M_{27} & M_{28} \\ M_{31} & M_{32} & M_{33} & M_{34} & M_{35} & M_{36} & M_{37} & M_{38} \\ M_{41} & M_{42} & M_{43} & M_{44} & M_{45} & M_{46} & M_{47} & M_{48} \\ M_{51} & M_{52} & M_{53} & M_{54} & M_{55} & M_{56} & M_{57} & M_{58} \\ M_{61} & M_{62} & M_{63} & M_{64} & M_{65} & M_{66} & M_{67} & M_{68} \\ M_{71} & M_{72} & M_{73} & M_{74} & M_{75} & M_{76} & M_{77} & M_{78} \\ M_{81} & M_{82} & M_{83} & M_{84} & M_{85} & M_{86} & M_{87} & M_{88} \end{pmatrix}$$

where,

$$\begin{aligned} M_{11} &= (-ie^{ik_F a} u + e^{ik_F a} u Z - e^{2ik_F a} u Z) \\ M_{12} &= 0 \\ M_{13} &= 0 \\ M_{14} &= -v(i e^{ik_F a} - Z + e^{ik_F a} Z) \\ M_{15} &= (i e^{ik_F a + i\varphi} u - e^{ik_F a + i\varphi} u Z + e^{2ik_F a + i\varphi} u Z) \\ M_{16} &= 0 \\ M_{17} &= 0 \\ M_{18} &= (i e^{ik_F a + i\varphi} v + e^{ik_F a + i\varphi} v Z - e^{i\varphi} v Z) \\ M_{21} &= 0 \\ M_{22} &= (i e^{ik_F a} u - e^{ik_F a} u Z + e^{2ik_F a} u Z) \\ M_{23} &= -v(i e^{ik_F a} - Z + e^{ik_F a} Z) \\ M_{24} &= 0 \\ M_{25} &= 0 \\ M_{26} &= (-i e^{ik_F a + i\varphi} u + e^{ik_F a + i\varphi} u Z - e^{2ik_F a + i\varphi} u Z) \\ M_{27} &= (i e^{ik_F a + i\varphi} v + e^{ik_F a + i\varphi} v Z - e^{i\varphi} v Z) \\ M_{28} &= 0 \\ M_{31} &= 0 \\ M_{32} &= (i e^{ik_F a} v - e^{ik_F a} v Z + e^{2ik_F a} v Z) \end{aligned}$$

$$\begin{aligned}
M_{33} &= -u(ie^{ik_{Fa}} - Z + e^{ik_{Fa}}Z) \\
M_{34} &= 0 \\
M_{35} &= 0 \\
M_{36} &= (-ie^{ik_{Fa}}v + e^{ik_{Fa}}vZ - e^{2ik_{Fa}}vZ) \\
M_{37} &= (ie^{ik_{Fa}}u - uZ + e^{ik_{Fa}}uZ) \\
M_{38} &= 0 \\
M_{41} &= (-ie^{ik_{Fa}}v + e^{ik_{Fa}}vZ - e^{2ik_{Fa}}vZ) \\
M_{42} &= 0 \\
M_{43} &= 0 \\
M_{44} &= -u(ie^{ik_{Fa}} - Z + e^{ik_{Fa}}Z) \\
M_{45} &= (ie^{ik_{Fa}}v - e^{ik_{Fa}}vZ + e^{2ik_{Fa}}vZ) \\
M_{46} &= 0 \\
M_{47} &= 0 \\
M_{48} &= (ie^{ik_{Fa}}u - uZ + e^{ik_{Fa}}uZ) \\
M_{51} &= (2e^{2ik_{Fa}}Jmm'u(i - 2Z) + 2e^{3ik_{Fa}}(-i + Jmm')uZ + 2e^{ik_{Fa}}(i + Jmm')u(-i + Z)) \\
M_{52} &= (e^{2ik_{Fa}}F_1F_2Ju(i - 2Z) + e^{3ik_{Fa}}F_1F_2JuZ + e^{ik_{Fa}}F_1F_2Ju(-i + Z)) \\
M_{53} &= (-F_1F_2JvZ - e^{2ik_{Fa}}F_1F_2Jv(i + Z) + e^{ik_{Fa}}F_1F_2Jv(i + 2Z)) \\
M_{54} &= (2e^{2ik_{Fa}}v(1 - iZ) + 2(i + Jmm')vZ + 2e^{2ik_{Fa}}Jmm'v(i + Z) - 2e^{ik_{Fa}}Jmm'v(i + 2Z)) \\
M_{55} &= -2e^{2ik_{Fa}+i\varphi}u \\
M_{56} &= 0 \\
M_{57} &= 0 \\
M_{58} &= -2e^{i(k_{Fa}+\varphi)}v \\
M_{61} &= (e^{2ik_{Fa}}F_1F_2Ju(i - 2Z) + e^{3ik_{Fa}}F_1F_2JuZ + e^{ik_{Fa}}F_1F_2Ju(-i + Z)) \\
M_{62} &= 2e^{ik_{Fa}}u(1 + (-1 + e^{ik_{Fa}})J(-1 + m)(1 + m')(i + (-1 + e^{ik_{Fa}})Z) + 2e^{ik_{Fa}}Z \sin(k_{Fa})) \\
M_{63} &= 2v((-i - J(-1 + m)(1 + m'))Z - e^{2ik_{Fa}}(-i + J(-1 + m)(1 + m'))(i + Z) + e^{ik_{Fa}}J(-1 + m)(1 + m')(i + 2Z)) \\
M_{64} &= (F_1F_2JvZ + e^{2ik_{Fa}}F_1F_2Jv(i + Z) - e^{ik_{Fa}}F_1F_2Jv(i + 2Z)) \\
M_{65} &= 0 \\
M_{66} &= -2e^{ik_{Fa}+i(k_{Fa}+\varphi)}u \\
M_{67} &= 2e^{i(k_{Fa}+\varphi)}v \\
M_{68} &= 0 \\
M_{71} &= e^{-ik_{Fa}}(e^{2ik_{Fa}}F_1F_2Jv(i - 2Z) + e^{3ik_{Fa}}F_1F_2JvZ + e^{ik_{Fa}}F_1F_2Jv(-i + Z)) \\
M_{72} &= 2v(-(-1 + e^{ik_{Fa}})J(-1 + m)(1 + m')(i + (-1 + e^{ik_{Fa}})Z) + i(i + (-1 + e^{2ik_{Fa}})Z)) \\
M_{73} &= e^{-ik_{Fa}}(2(i + J(m - 1)(m' + 1))uZ + 2e^{2ik_{Fa}}(-i + J(m - 1)(m' + 1))u(i + Z) - 2e^{ik_{Fa}}J(m - 1)(m' + 1)u(i + 2Z)) \\
M_{74} &= e^{-ik_{Fa}}(F_1F_2JuZ + e^{2ik_{Fa}}F_1F_2Ju(i + Z) - e^{ik_{Fa}}F_1F_2Ju(i + 2Z)) \\
M_{75} &= 0 \\
M_{76} &= 2e^{ik_{Fa}}v \\
M_{77} &= -2u \\
M_{78} &= 0 \\
M_{81} &= e^{-ik_{Fa}}(2e^{ik_{Fa}}v(1 + iZ) + 2e^{3ik_{Fa}}(-i + Jmm')vZ + 2e^{ik_{Fa}}Jmm'v(-i + Z) - 2e^{2ik_{Fa}}Jmm'v(-i + 2Z)) \\
M_{82} &= e^{-ik_{Fa}}(-e^{2ik_{Fa}}F_1F_2Jv(i - 2Z) - e^{3ik_{Fa}}F_1F_2JvZ - e^{ik_{Fa}}F_1F_2Jv(-i + Z)) \\
M_{83} &= e^{-ik_{Fa}}(F_1F_2JuZ + e^{2ik_{Fa}}F_1F_2Ju(i + Z) - e^{ik_{Fa}}F_1F_2Ju(i + 2Z)) \\
M_{84} &= e^{-ik_{Fa}}(2(i + Jmm')uZ + 2e^{2ik_{Fa}}(-i + Jmm')u(i + Z) - 2e^{ik_{Fa}}Jmm'u(i + 2Z)) \\
M_{85} &= -2e^{ik_{Fa}}v \\
M_{86} &= 0 \\
M_{87} &= 0 \\
M_{88} &= -2u
\end{aligned}$$

APPENDIX B: EXPLICIT FORM OF ANDREEV BOUND STATES

The explicit form of $A(\varphi)$, $B(\varphi)$, C in Andreev bound state expression is given by

$$\begin{aligned}
A(\varphi) = & -2e^{3ik_F a}((1+2Z^2)(8(1+2Z^2)^2+J^4(F_2^2+m'+m'^2)^2(1+10(Z^2+Z^4))+J^2(3+6m'(1+m')+8Z^2 \\
& +2(F_2^2-8(F_2^2+m'+m'^2)Z^2-4(-1+2F_2^2+2m'(1+m'))Z^4))) +2Z^2(1+2Z^2)(16+16J^3(F_2^2+m'+m'^2)Z \\
& -16Z^2+3J^4(F_2^2+m'+m'^2)^2(-1+Z^2)+4J^2(-1+2F_2^2+2m'(1+m'))(-1+Z^2)) \cos(2k_F a) -2Z^3(16Z(-3+Z^2) \\
& +J^4(F_2^2+m'+m'^2)^2Z(-3+Z^2)+4J^2(-1+2F_2^2+2m'(1+m'))Z(-3+Z^2)+16J(-1+3Z^2)+4J^3(F_2^2+m' \\
& +m'^2)(-1+3Z^2)) \cos(3k_F a) +8 \cos(\varphi) + (16Z^2-J^2(-1+2F_2^2-2m'(1+m'))(1+2Z^2)) \cos(\varphi) +2Z \cos(k_F a)(8Z \\
& +12J(1+2Z^2)^2+J^2Z(-3-2F_2^2-6m'(1+m')-4Z^2+8(F_2^2+m'+m'^2)Z^2+4(-1+2F_2^2+2m'(1+m'))Z^4) \\
& +16(Z^3+Z^5)-4J^3(F_2^2+m'+m'^2)(1+5(Z^2+Z^4))-3J^4(F_2^2+m'+m'^2)^2Z(1+5(Z^2+Z^4)))+(8Z+J(4 \\
& +J(-1+2F_2^2-2m'(1+m'))Z)) \cos(\varphi) +2Z(-8+12JZ(1+2Z^2)^2-16(Z^2+Z^4)+J^2(3+2F_2^2+6m'(1+m') \\
& +4Z^2-8(F_2^2+m'+m'^2)Z^2-4(-1+2F_2^2+2m'(1+m'))Z^4)+3J^4(F_2^2+m'+m'^2)^2(1+5(Z^2+Z^4)) \\
& -4J^3(F_2^2+m'+m'^2)Z(1+5(Z^2+Z^4)))+(-8+J^2(1-2F_2^2+2m'(1+m'))+4JZ) \cos(\varphi) \sin(k_F a) \\
& -4Z^2(1+2Z^2)(-16Z+J^2(-4Z+(F_2^2+m'+m'^2)(8Z+J(4+3J(F_2^2+m'+m'^2)Z-4Z^2)))) \sin(2k_F a) \\
& -2Z^3(16-48Z^2+16JZ(-3+Z^2)+4J^3(F_2^2+m'+m'^2)Z(-3+Z^2)-J^4(F_2^2+m'+m'^2)^2(-1+3Z^2) \\
& -4J^2(-1+2F_2^2+2m'(1+m'))(-1+3Z^2)) \sin(3k_F a)
\end{aligned}$$

$$\begin{aligned}
B(\varphi) = & -2J^2e^{6ik_F a}(-64F_2^4J^2(1+6(Z^2+Z^4))-3(1+2m')^2(32(Z^2+Z^4)+J^2(1+6(Z^2+Z^4)))) +4F_2^2(-J^2(5 \\
& +4m'(1+m'))(1+6(Z^2+Z^4))-16(1+8(Z^2+Z^4))) +4J^2 \cos(\varphi) +16F_2^2J^2 \cos(\varphi) -64F_2^4J^2 \cos(\varphi) \\
& +16J^2m' \cos(\varphi) +16J^2m'^2 \cos(\varphi) +128Z^2 \cos(\varphi) +512F_2^2Z^2 \cos(\varphi) +24J^2Z^2 \cos(\varphi) +96F_2^2J^2Z^2 \cos(\varphi) \\
& -384F_2^4J^2Z^2 \cos(\varphi) +512m'Z^2 \cos(\varphi) +96J^2m'Z^2 \cos(\varphi) +512m'^2Z^2 \cos(\varphi) +96J^2m'^2Z^2 \cos(\varphi) \\
& +128Z^4 \cos(\varphi) +512F_2^2Z^4 \cos(\varphi) +24J^2Z^4 \cos(\varphi) +96F_2^2J^2Z^4 \cos(\varphi) -384F_2^4J^2Z^4 \cos(\varphi) \\
& +512m'Z^4 \cos(\varphi) +96J^2m'Z^4 \cos(\varphi) +512m'^2Z^4 \cos(\varphi) +96J^2m'^2Z^4 \cos(\varphi) -8JZ(1+2Z^2) \cos(k_F a) \\
& (-8F_2^2-(1+2m')^2+(1+2m')^2 \cos(\varphi))(-4+JZ+4F_2^2JZ+(4+(-1+4F_2^2)JZ) \cos(\varphi)) +4Z^2 \cos(2k_F a) \\
& (-8F_2^2-(1+2m')^2+(1+2m')^2 \cos(\varphi))(16-16JZ-16Z^2+(1+4F_2^2)J^2(-1+Z^2)+(16JZ+16(-1+Z^2) \\
& +(-1+4F_2^2)J^2(-1+Z^2)) \cos(\varphi)) +64F_2^2 \cos(2\varphi)J^2 \cos(2\varphi) +4F_2^2J^2 \cos(2\varphi) -4J^2m' \cos(2\varphi) \\
& +16F_2^2J^2m' \cos(2\varphi) -4J^2m'^2 \cos(2\varphi) +16F_2^2J^2m'^2 \cos(2\varphi) -32Z^2 \cos(2\varphi) -6J^2Z^2 \cos(2\varphi) \\
& +24F_2^2J^2Z^2 \cos(2\varphi) -128m'Z^2 \cos(2\varphi) -24J^2m'Z^2 \cos(2\varphi) +96F_2^2J^2m'Z^2 \cos(2\varphi) -128m'^2Z^2 \cos(2\varphi) \\
& -24J^2m'^2Z^2 \cos(2\varphi) +96F_2^2J^2m'^2Z^2 \cos(2\varphi) -32Z^4 \cos(2\varphi) -6J^2Z^4 \cos(2\varphi) +24F_2^2J^2Z^4 \cos(2\varphi) \\
& -128m'Z^4 \cos(2\varphi) -24J^2m'Z^4 \cos(2\varphi) +96F_2^2J^2m'Z^4 \cos(2\varphi) -128m'^2Z^4 \cos(2\varphi) -24J^2m'^2Z^4 \cos(2\varphi) \\
& +96F_2^2J^2m'^2Z^4 \cos(2\varphi) +8JZ(1+2Z^2)(-8F_2^2-(1+2m')^2+(1+2m')^2 \cos(\varphi))(J+4F_2^2J+4Z+(-J \\
& +4F_2^2J-4Z) \cos(\varphi)) \sin(k_F a) -8Z^2(-8F_2^2-(1+2m')^2+(1+2m')^2 \cos(\varphi))(-16Z+J(-4+Z(J+4F_2^2J+4Z)) \\
& + (16Z+J(4+(-1+4F_2^2)JZ-4Z^2)) \cos(\varphi)) \sin(2k_F a)
\end{aligned}$$

$$\begin{aligned}
C = & e^{3ik_F a}(-1-2Z^2+2Z^2 \cos(k_F a)-2Z \sin(k_F a))(4J^2(1+2F_2^2+2m'(1+m')+2Z^2-4(F_2^2+m'+m'^2)Z^2-2(-1+2F_2^2 \\
& +2m'(1+m'))Z^4)+16(1+6(Z^2+Z^4))+J^4(F_2^2+m'+m'^2)^2(1+6(Z^2+Z^4))+2Z(-2(-4+J^2(F_2^2+m'+m'^2)) \\
& (1+2Z^2)(4Z+J(2+J(F_2^2+m'+m'^2)Z)) \cos(k_F a)+Z(4(-1+Z)+J(J(F_2^2+m'+m'^2)(-1+Z)+2(1+Z))) \\
& (4(1+Z)+J(2-2Z+J(F_2^2+m'+m'^2)(1+Z)))) \cos(2k_F a) +2(-4+J^2(F_2^2+m'+m'^2))(4+J(J(F_2^2+m'+m'^2) \\
& -2Z))(1+2Z^2) \sin(k_F a) +2Z(-4+J(-J(F_2^2+m'+m'^2)+2Z))(4Z+J(2+J(F_2^2+m'+m'^2)Z)) \sin(2k_F a))
\end{aligned}$$

APPENDIX C

TABLE I: Spin flip probability (F_2) values of the HSM for different S and m'

S	m'	F_2	S	m'	F_2	S	m'	F_2	S	m'	F_2
$\frac{1}{2}$	$-\frac{1}{2}$	1	$\frac{11}{2}$	$-\frac{11}{2}$	$\sqrt{11}$	$\frac{15}{2}$	$-\frac{15}{2}$	$\sqrt{15}$	$\frac{19}{2}$	$-\frac{19}{2}$	$\sqrt{19}$
	$\frac{1}{2}$	0		$-\frac{9}{2}$	$2\sqrt{5}$		$-\frac{13}{2}$	$2\sqrt{7}$		$-\frac{17}{2}$	6
$\frac{3}{2}$	$-\frac{3}{2}$	$\sqrt{3}$		$-\frac{7}{2}$	$3\sqrt{3}$		$-\frac{11}{2}$	$\sqrt{39}$		$-\frac{15}{2}$	$\sqrt{51}$
	$-\frac{1}{2}$	2		$-\frac{5}{2}$	$4\sqrt{2}$		$-\frac{9}{2}$	$4\sqrt{3}$		$-\frac{13}{2}$	8
	$\frac{1}{2}$	$\sqrt{3}$		$-\frac{3}{2}$	$\sqrt{35}$		$-\frac{7}{2}$	$\sqrt{55}$		$-\frac{11}{2}$	$5\sqrt{3}$
	$\frac{3}{2}$	0		$-\frac{1}{2}$	6		$-\frac{5}{2}$	$2\sqrt{15}$		$-\frac{9}{2}$	$2\sqrt{21}$
$\frac{5}{2}$	$-\frac{5}{2}$	$\sqrt{5}$		$\frac{1}{2}$	$\sqrt{35}$		$-\frac{3}{2}$	$3\sqrt{7}$		$-\frac{7}{2}$	$\sqrt{91}$
	$-\frac{3}{2}$	$2\sqrt{2}$		$\frac{3}{2}$	$4\sqrt{2}$		$-\frac{1}{2}$	8		$-\frac{5}{2}$	$4\sqrt{6}$
	$-\frac{1}{2}$	3		$\frac{5}{2}$	$3\sqrt{3}$		$\frac{1}{2}$	$3\sqrt{7}$		$-\frac{3}{2}$	$3\sqrt{11}$
	$\frac{1}{2}$	$2\sqrt{2}$		$\frac{7}{2}$	$2\sqrt{5}$		$\frac{3}{2}$	$2\sqrt{15}$		$-\frac{1}{2}$	10
	$\frac{3}{2}$	$\sqrt{5}$		$\frac{9}{2}$	$\sqrt{11}$		$\frac{5}{2}$	$\sqrt{55}$		$\frac{1}{2}$	$3\sqrt{11}$
	$\frac{5}{2}$	0		$\frac{11}{2}$	0		$\frac{7}{2}$	$4\sqrt{3}$		$\frac{3}{2}$	$4\sqrt{6}$
$\frac{7}{2}$	$-\frac{7}{2}$	$\sqrt{7}$	$\frac{13}{2}$	$-\frac{13}{2}$	$\sqrt{13}$		$\frac{9}{2}$	$\sqrt{39}$		$\frac{5}{2}$	$\sqrt{91}$
	$-\frac{5}{2}$	$2\sqrt{3}$		$-\frac{11}{2}$	$2\sqrt{6}$		$\frac{11}{2}$	$2\sqrt{7}$		$\frac{7}{2}$	$2\sqrt{21}$
	$-\frac{3}{2}$	$\sqrt{15}$		$-\frac{9}{2}$	$\sqrt{33}$		$\frac{13}{2}$	$\sqrt{15}$		$\frac{9}{2}$	$5\sqrt{3}$
	$-\frac{1}{2}$	4		$-\frac{7}{2}$	$2\sqrt{10}$		$\frac{15}{2}$	0		$\frac{11}{2}$	8
	$\frac{1}{2}$	$\sqrt{15}$		$-\frac{5}{2}$	$3\sqrt{5}$	$\frac{17}{2}$	$-\frac{17}{2}$	$\sqrt{17}$		$\frac{13}{2}$	$\sqrt{51}$
	$\frac{3}{2}$	$2\sqrt{3}$		$-\frac{3}{2}$	$4\sqrt{3}$		$-\frac{15}{2}$	$4\sqrt{2}$		$\frac{15}{2}$	6
	$\frac{5}{2}$	$\sqrt{7}$		$-\frac{1}{2}$	7		$-\frac{13}{2}$	$3\sqrt{5}$		$\frac{17}{2}$	$\sqrt{19}$
	$\frac{7}{2}$	0		$\frac{1}{2}$	$4\sqrt{3}$		$-\frac{11}{2}$	$2\sqrt{14}$		$\frac{19}{2}$	0
$\frac{9}{2}$	$-\frac{9}{2}$	3		$\frac{3}{2}$	$3\sqrt{5}$		$-\frac{9}{2}$	$\sqrt{65}$			
	$-\frac{7}{2}$	4		$\frac{5}{2}$	$2\sqrt{10}$		$-\frac{7}{2}$	$6\sqrt{2}$			
	$-\frac{5}{2}$	$\sqrt{21}$		$\frac{7}{2}$	$\sqrt{33}$		$-\frac{5}{2}$	$\sqrt{77}$			
	$-\frac{3}{2}$	$2\sqrt{6}$		$\frac{9}{2}$	$2\sqrt{6}$		$-\frac{3}{2}$	$4\sqrt{5}$			
	$-\frac{1}{2}$	5		$\frac{11}{2}$	$\sqrt{13}$		$-\frac{1}{2}$	9			
	$\frac{1}{2}$	$2\sqrt{6}$		$\frac{13}{2}$	0		$\frac{1}{2}$	$4\sqrt{5}$			
	$\frac{3}{2}$	$\sqrt{21}$					$\frac{3}{2}$	$\sqrt{77}$			
	$\frac{5}{2}$	4					$\frac{5}{2}$	$6\sqrt{2}$			
	$\frac{7}{2}$	3					$\frac{7}{2}$	$\sqrt{65}$			
	$\frac{9}{2}$	0					$\frac{9}{2}$	$2\sqrt{14}$			
							$\frac{11}{2}$	$3\sqrt{5}$			
							$\frac{13}{2}$	$4\sqrt{2}$			
							$\frac{15}{2}$	$\sqrt{17}$			
							$\frac{17}{2}$	0			

* colin.nano@gmail.com

- ¹ T. Takui in “Molecular Magnetism” K.Itoh, M. Kinoshita (eds) Kodansha and Gordon and Breach, Tokyo 2000.
- ² D. Gatteschi and R. Sessoli, *Angew. Chem. Int. Ed.* 42, 268 (2003).
- ³ W. Wernsdorfer, et. al., *Phys. Rev. B* 65, 180403(R) (2002).
- ⁴ D. Aravena, D. Venegas-Yazigi & E. Ruiz, *Scientific Reports* 6, Article number: 23847 (2016).
- ⁵ Herr, A. Y. & Herr, Q. P. Josephson magnetic random access memory system and method. US Patent 8,270,209 (2012).
- ⁶ Holmes, D. S., Ripple, A. L. & Manheimer, M. A. Energy-efficient superconducting computing-power budgets and requirements. *IEEE Trans. Appl. Supercond.* 23, 1701610 (2013).
- ⁷ E. C. Gingrich, et. al., Controllable $0 - \pi$ Josephson junctions containing a ferromagnetic spin valve, *Nature Physics* 12, 564- 567 (2016).
- ⁸ A. K. Feofanov, et. al., Implementation of superconductor/ferromagnet/ superconductor π -shifters in superconducting digital and quantum circuits, *Nature Physics* 6, 593-597 (2010).
- ⁹ Ryazanov, V. V. et al. Coupling of two superconductors through a ferromagnet: Evidence for a π -junction. *Phys. Rev. Lett.* 86, 2427-2430 (2001).
- ¹⁰ Van Harlingen, D. J. Phase-sensitive tests of the symmetry of the pairing state in the high-temperature superconductors-evidence for $d_{x^2-y^2}$ symmetry. *Rev. Mod. Phys.* 67, 515-535 (1995).
- ¹¹ Philip F. Bagwell, *Phys. Rev. B* 46, 12573 (1992).
- ¹² A. Krichevsky, M. Schechter, Y. Imry, and Y. Levinson, *Phys. Rev. B* 61, 3723 (2000).
- ¹³ Firoz Islam and Colin Benjamin, *J. Phys.: Condens. Matter* 28 (2016) 035305.
- ¹⁴ Burzuri et al., *J. Phys.: Condens. Matter* 27, 113202 (2015).
- ¹⁵ G. Annuziata, H. Enoksen, J. Linder, M. cuoco, C. Noce and A. Sudbo, *Phys. Rev. B* 83, 144520 (2011).
- ¹⁶ Henrik Enoksen , Jacob Linder and Asle Sudbo, *Phys Rev B* 85,014512 (2012).
- ¹⁷ O. L. T. de Menezes and J. S. Helman, *American Journal of Physics* 53, 1100 (1985).
- ¹⁸ A. Furusaki and M. Tsukuda, *Solid state Commun.* 78, 299 (1991).
- ¹⁹ C. W. J. Beenakker, *Phys. Rev. Lett.* 67, 3836 (1991).
- ²⁰ A. A. Golubov, M. Y. Kupriyanov, and E. Il'ichev, *Rev. Mod. Phys.* 76, 411 (2004).
- ²¹ A. Furusaki, H. Takayanagi, and M. Tsukada, *Phys. Rev. Lett.* 67, 132 (1991); *Phys. Rev. B* 45, 10563 (1992).
- ²² C. Benjamin et al., Controllable π junction in a Josephson quantum-dot device with molecular spin, *European Physical Journal B* 57 279 (2007).
- ²³ L. B. Ioffe et al., Quiet SDS Josephson Junctions for Quantum Computing, *Nature* 398, 679 (1999); A. L. Fauchere, Ph. D thesis, Theoretische Physik, ETH-Zurich, Switzerland (1999).
- ²⁴ E. Il'ichev et. al., Degenerate Ground State in a Mesoscopic $YBa_2Cu_3O_{7-x}$ Grain Boundary Josephson Junction, *Phys. Rev. Lett.* 86, 5369 (2001).
- ²⁵ H. T. Man, T.M. Klapwijk, and A. F. Morpurgo, arXiv:cond-mat/0504566 (unpublished).
- ²⁶ R. Mélin, C. Benjamin, and T. Martin, *Phys. Rev. B* 77, 094512 (2008).